Title

Macrophages promote epithelial proliferation following infectious and non-infectious lung injury through a Trefoil factor 2-dependent mechanism

Journal

Mucosal Immunology, 12(1)

ISSN

1933-0219

Authors

Hung, Li-Yin
Sen, Debasish
Oniskey, Taylor K
et al.

Publication Date

2019

DOI

10.1038/s41385-018-0096-2

Peer reviewed

Published in final edited form as:

Mucosal Immunol. 2019 January ; 12(1): 64–76. doi:10.1038/s41385-018-0096-2.

Macrophages promote epithelial proliferation following infectious and non-infectious lung injury through a Trefoil factor 2-dependent mechanism

Li-Yin Hung[1], **Debasish Sen**[6], **Taylor K. Oniskey**[1], **Jeremey Katzen**[4], **Noam A. Cohen**[3], **Andrew E. Vaughan**[2], **Wildaliz Nieves**[1], **Anatoly Urisman**[6], **Michael F. Beers**[4,5], **Matthew F. Krummel**[6], and **De'Broski R. Herbert**[1]

[1]Department of Pathobiology, University of Pennsylvania School of Veterinary Medicine, Philadelphia, PA 19104

[2]Department of Biological Sciences, University of Pennsylvania School of Veterinary Medicine, Philadelphia, PA 19104

[3]Departments of Otorhinolaryngology—Head and Neck Surgery, University of Pennsylvania Perelman School of Medicine, Monell Chemical Senses Center, and Philadelphia VA Medical Center Surgical Service

[4]Pulmonary, Allergy, and Critical Care Division, Department of Medicine, Perelman School of Medicine, University of Pennsylvania, Philadelphia, Pennsylvania

[5]PENN Center for Pulmonary Biology, University of Pennsylvania, Perelman School of Medicine, Philadelphia, Pennsylvania

[6]Department of Pathology, University of California, San Francisco, San Francisco, CA 94143, USA.

Abstract

Coordinated efforts between macrophages and epithelia are considered essential for wound healing, but the macrophage-derived molecules responsible for repair are poorly defined. This work demonstrates that lung macrophages rely upon Trefoil factor 2 to promote epithelial proliferation following damage caused by sterile wounding, *Nippostrongylus brasiliensis* or Bleomycin sulfate. Unexpectedly, the presence of T, B, or ILC populations was not essential for macrophage-driven repair. Instead, conditional deletion of TFF2 in myeloid-restricted $CD11c^{Cre}$ TFF2 flox mice exacerbated lung pathology and reduced the proliferative expansion of $CD45^{-}$ $EpCAM^{+}$ pro-SPC^{+} alveolar type 2 cells. TFF2 deficient macrophages had reduced expression of the Wnt genes *Wnt4* and *Wnt16* and reconstitution of hookworm-infected $CD11c^{Cre}$ TFF2 flox mice with rWnt4 and Wnt16 restored the proliferative defect in lung epitheliapost-injury. These

Corresponding Author: De'Broski R. Herbert Ph.D., 3800 Spruce St. Old Vet369E, Philadelphia, PA 19104, Tel: (215) 898-9151, Fax (215) 206-8091, debroski@vet.upenn.edu.

Author contributions

L.-Y.H., D.S., T.K.O., J.K., and W.N. performed experiments, L.-Y.H., D.S., T.K.O., W.N., M.F.B, M.F.K., N.A.C., A.E.V. and D.R.H, analyzed data, D.R.H. conceived the study and D.R.H, N.A.C., A.E.V. and L.-Y.H wrote the manuscript.

data reveal a previously unrecognized mechanism wherein lung myeloid phagocytes utilize a TFF2/Wnt axis as a mechanism that drives epithelial proliferation following lung injury.

Introduction

Tissue injury is inevitable, making regeneration fundamental to evolutionary fitness. Regeneration of epithelia following lung tissue damage is particularly important, because proximal (airway) and distal (alveolar) compartments form a dynamic barrier against environmental stimuli [1]. Alveolar gas exchange function is under constant threat from inspired air containing potentially harmful chemical, mechanical, and infectious agents. Damage-induced loss of alveolar type I cells (ATI) would impair lung function, if not replenished by distal lung stem cells[2–4]. Even though the yolk-sac derived alveolar macrophages (AM) are a major constituent of distal lung tissue, whether AM or myeloid cells in general are important drivers of epithelial replenishment following lung injury is poorly understood[5, 6].

Classification of tissue macrophages (M_φ) into classically activated (M1) or alternatively activated (M2) subsets only partially defines M_φ heterogeneity[7, 8]. Type 2 cytokines (e.g. interleukin 4 and 13) induce M2 cells that regulate pathogenic inflammation[9] and purportedly drive repair, but there is scant evidence showing that M2 cells induce epithelial cell proliferation[10, 11]. M2 secreted factors include: Amcase, Arginase I, chitinase-like proteins (Ym1/Ym2), resistin-like molecule alpha (Relm-$_\alpha$), interleukin 10 and transforming growth factor beta (TGF-$_\beta$), all of which are immunoregulatory, but not necessarily regenerative[12]. In certain contexts, M_φ secrete Wingless-Int (Wnt) glycoproteins[13, 14], a family of regenerative molecules controlling epithelial cell proliferation, differentiation, and polarity[15]. Wnt's function through Frizzled receptors for β-catenin-dependent transcription[16], but also signal through noncanonical pathways that rely upon calcium/calmodulin-dependent protein kinases (e.g. Camkk2b). Irrespective of the pathway engaged, whether specific cytokines or epithelial secreted factors induce Mφ to produce Wnt's or other epithelial regenerative molecules is unknown.

Trefoil factor family (TFF1, TFF2, TFF3) molecules are small, reparative cytokines (6–18 kDa) that promote rapid movement of epithelia over denuded basement membrane[17]. Mouse strains deficient for *Tff1, Tff2*, or *Tff3* possess constitutive defects in gastrointestinal (GI) barrier function[18–20], but the critical source(s) and function(s) for TFF's in non-GI tissues are unclear. Even though *Tff2* can be produced by gastric epithelia, peritoneal macrophages and splenic T lymphocytes[21], how this molecule regulates epithelial repair is understudied. *Tff2* deficiency in all of its potential cellular sources exacerbated lung damage caused by the murine hookworm *Nippostrongylus brasiliensis* (*N.b.*), and recent data shows that both BM-derived and nonBM-derived TFF2 drives repair [22, 23]. Moreover, recent demonstration that myeloid cells influenced by Type 2 immune responses (i.e. IL-4Ralpha signaling) regenerate lung following partial pneumonectomy[24], prompted speculation that Mφ could repair damaged lung tissue by producing TFF2.

This study demonstrates myeloid-specific deletion of TFF2 impairs epithelial proliferation in three different models of lung injury. Surprisingly, we found no evidence for interleukin 4

receptor alpha (IL-4Rα) expression in lung repair, suggesting the classical model of M2 polarization as pro-reparative is extremely context dependent[10]. Recombination activating gene/common gamma c chain deficient (RAGγc$^{-/-}$) animals also had no defects in epithelial proliferation post-injury, indicating that neither adaptive lymphocytes or ILC were required in these systems. Instead, macrophages could directly promote epithelial proliferation in the absence of other cell types in a co-culture system containing either tracheal or alveolar type 2 cells (AT2). One demonstrated mechanism was that myeloid-intrinsic TFF2 was required for myeloid-derived Wnt gene expression (*Wnt4* and *Wnt16*). Indeed, Wnt protein administration restored AT2 proliferation in myeloid-specific TFF2 mutants. This work supports a model wherein myeloid-epithelial cell interactions induce epithelial cell proliferation to restore damaged pulmonary tissue.

RESULTS

Proliferation of lung epithelia following hookworm-induced injury depends on the presence of lung macrophages.

En route to the intestine, migratory hookworm larvae transiently damage alveolar architecture[25], but how pulmonary tissue repairs is unknown. Type 2 cytokines such as IL-4 and IL-13 are considered key mediators of wound healing, at least in part, through driving M2 macrophage polarization[12]. *N.b.* infection causes a transient petechial lung injury that peaks by d3 and resolves by d9 (Figure 1a), therefore we postulated that M2 proliferative expansion was prerequisite for repair of *N.b.*-damaged lungs, as IL-4 drives Mφ proliferation *in situ*[26,27]. Immunofluorescence lung tissue staining for Chitinase like 3/Ym1 (a M2 marker)[10] and Ki-67 (cell-cycle protein) were used to decipher whether M2 cells underwent proliferative expansion following hookworm injury (Figure 1c and Supplemental Fig 1a-b). Data show that from pre-infection to d9 post-infection the overall Ki-67^{+} cell numbers accumulated during the course of infection while numbers of Ym1^{+} cells remained somewhat similar (Figure 1b and c). Proliferating Mφ, (Ym1^{+}/Ki-67^{+}) were detected between d3–9, but most of the Ki67^{+} cells in the lung did not co-express Ym1 (Figure 1b-e). Thus, contrary to expectation, most of the proliferating cells within hookworm-damaged lungs were not M2 cells.

We asked whether the non-myeloid cells that were Ki-67^{+} were epithelial cells because hookworm infection causes a defect in pulmonary gas exchange[28]. To determine whether lung epithelia were indeed entering the S-phase during the recovery from hookworm-injury, we devised a flow cytometry strategy (Supplemental Fig 1c) that utilized either an EdU or BrdU pulse at 24h prior to euthanasia on different days post-infection (d0,1, 3, 5, 7, and 9) followed by identification of cells that were (BrdU^{+}, CD45^{-}, EpCAM^{+}) using flow cytometry. Data show that the percentages of BrdU^{+}, EpCAM^{+} cells increased 3-fold over baseline at d3 and 19-fold between d5–7 post-infection (Figure 1f-g). Strikingly, the infection-induced increase in proliferating epithelia was unabated in IL-4Rα$^{-/-}$ and recombination activating gene 1/common gamma c chain (RAGγc$^{-/-}$) deficient strains (Figure 1h). These data indicated that the proliferative expansion of epithelia following *N.b.* infection did not require IL-4/IL-13 responsiveness, T, B, or ILC populations.

To address whether local tissue Mφ regulated epithelial proliferation in the damaged lung tissue, mice were generated to co-express the reverse tetracycline-controlled transactivator (rtTA) under control of the human CD68 promoter with a diphtheria toxin A transgene under control of the tetracycline operator (TetO-DTA). This strain (referred to as CD68-DTA) was compared to single transgenic CD68rtTA controls (CD68). The specificity and duration of Mφ deletion in this strain following systemic tetracycline administration has been previously described[29]. To confirm that lung Mφ depletion could be achieved during *N.b.* infection, CD68 and CD68-DTA mice were administered 250 ng intranasal (i.n.) anhydrotetracyline (Ahtet) on day's −4, −2, 0 and 2 post-infection. Analysis at d4 post-infection demonstrated selective deletion of two populations within lung digests: a) auto-fluorescent, $CD11c^{+}$, Siglec-F^{+} and b) $CD11b^{low/med}$, $MHCII^{+}$, $CD103^{-}$ cells, indicating selective depletion of AM and interstitial macrophages (IM), respectively (Figure 2a and b). Using this Mφ depletion protocol, data showed that in comparison to CD68 controls, proliferating SPC^{+} epithelia (ATII cells) in parasitized CD68-DTA mice were 3-fold reduced by d3 and 4-fold reduced between d5-d7 post-infection (Figure 2c-d). Lung Mφ depletion had no impact upon worm expulsion from the intestine (**data not shown**).

Next, blood oxygen content (SpO_2) was measured to determine if lung Mφ affected the ΔSpO_2 levels at d3–9 post-infection. Data show that although the d3 SpO_2 nadir was equivalent between strains, CD68 controls rapidly recovered following worm egress, whereas CD68-DTA mice remained 10% lower than baseline at both d7 and d9 (Figure 2e), indicating an important role for Mφ in promoting lung repair following hookworm infection.

Lung TFF2 expression is induced by hookworm infection in the absence of IL-4 receptor

Mφ can be a direct source of various repair proteins[13, 14] and since *Tff2* was induced in *N. brasiliensis*-infected lungs in the absence of IL-4Rα signaling (Supplementary Figure 1e), subsequent experiments addressed whether myeloid-derived TFF2 was involved in lung repair. TFF2 conditionally deficient mice on a C57BL/6 background were generated by expressing an internal ribosomal entry site-fluorescent tandem dimer (td)-Tomato cassette (IRES-TdTomato) immediately following the stop codon in exon 4 of *Tff2*, with two *loxP* sites flanking exons 2 and 3'UTR (Figure 3a and Supplementary Figure 2a). TFF2-tdTomato flox mice (designated "Tre-Tom") had no gross abnormalities and were born at the expected female:male ratios. Site-specific recombination and germ-line transmission were confirmed by Southern blot (Supplementary Figure 2b). As expected, *Tff2* mRNA was constitutively expressed in a small population of Td-$tomato^{+}$ gastric epithelial cells sorted from the stomach tissue of naive Tre-tom mice (Supplementary Figure 2c and data not shown), which was consistent with *Tff2* expression in the stomach[30].

To evaluate the *Tff2* expression in the pulmonary compartment, 300μm sections of agarose-filled lung tissue were prepared using established methods [31] and subjected to confocal imaging under steady-state and infectious conditions. Whereas baseline Td-tomato expression was sparse, but punctate within the distal lung compartment under steady-state conditions (Figure 3b), there were large, focal aggregates of Td-$Tomato^{+}$ cells within the alveolar compartment at d4 following hookworm infection (Figure 3c-d). These data indicated that infection-induced an increase of TFF2 expression occurred within large cells

in the alveoli. Based on their morphology and location, we hypothesized that some of these large TFF2 positive cells were of a hematopoietic lineage.

CD11c-mediated TFF2 deletion impairs epithelial proliferation following infectious lung injury

CD11c^{Cre}TFF2^{flox} mice were generated through intercross between Tretom and CD11c^{Cre} strains to test whether myeloid-derived TFF2 was biologically important[32]. Real-time PCR was used to compare *Tff2* mRNA transcript levels between TFF2 deficient, CD11c^{Cre}TFF2^{flox} and CD11c^{Cre} controls in 4 distinct FACS-sorted lung populations: lung epithelia (CD45^{-}EpCAM^{+}), AM (CD64^{+}, CD11b^{-}, CD11c^{+}), IM (CD64^{+}. CD11b^{+}, CD11c^{-}), and CD103^{+}DC (CD64^{-}, CD103^{+}, CD11c^{+}). (Gating strategy for the cell sorting is shown in (Supplementary Figure 3a). Results show that AM underwent infection-induced *Tff2* expression by d4 post-infection (Figure 3e and f). TFF2 was also evident in CD103 DC and interstitial macrophages and expression was lost in CD11c^{Cre}TFF2^{flox} mice (Supplementary Figure 3b). Curiously, *Tff2* transcripts were higher in lung epithelia sorted from CD11c^{Cre}TFF2^{flox} mice than epithelia in CD11c^{Cre} controls (Figure 3e and f), suggesting a compensatory *Tff2* upregulation in epithelial cells due to deletion in the myeloid compartment.

CD11c^{Cre}TFF2^{flox} mice had a reduced percentage of BrdU^{+} cells within alveolar type 2 cell populations (CD45^{-}. EpCAM^{+}, pro-SPC^{+}) when compared to CD11c^{Cre} controls at day 9 post-infection (Figure 3g and Supplementary Fig 4a). SpO_2 levels were significantly lower in CD11c^{Cre}TFF2^{flox} mice at d9 post-infection, implying a defect in lung function rebound (Figure 3h). Concerning the initial injury caused by larvae, the BAL RBC numbers were increased at day 3, reflective of more severe injury in CD11c^{Cre}TFF2^{flox} mice compared to CD11c^{Cre} controls (Supplementary Figure 4b). The alveolar space within infected CD11c^{Cre}TFF2^{flox} mice was markedly larger than CD11c^{Cre} controls evidenced by areas of enlarged airspace (Figure 3i) suggesting that resolution of hookworm injury that was abnormal in CD11c^{Cre}TFF2^{flox} mice.

Next, the bleomycin model of lung injury was used to determine whether myeloid-derived TFF2 was important for lung repair in a non-infectious context lacking excess Type 2 cytokine production[33]. Acute cytotoxicity of bleomycin causes severe alveolar cell damage, transient weight loss, pulmonary inflammation, and chronic collagen accumulation[2]. Bleomycin treatment transiently increased BAL TFF2 levels in both mouse strains, whereas CD11c^{Cre} controls underwent a 3-fold increase at d9, this early induction was reduced by myeloid-specific TFF2 deficiency (Figure 4a). On the other hand, CD11c^{Cre}TFF2^{flox} mice produced higher TFF2 levels than CD11c^{Cre} controls by d16, suggestive of compensatory production from a non-myeloid source at later stages when fibrosis occurs (Figure 4a). CD11c^{Cre}TFF2^{flox} animals experienced a transient, but significantly greater weight loss than CD11c^{Cre} controls during the acute injury phase, but subsequently recovered in the latter phase (Figure 4b). At day 9, the total protein levels in BAL fluid is higher in CD11c^{Cre} TFF2^{flox} (Figure 4c); also, the CD45^{-} EpCAM^{+} BrdU^{+} pro-SPC^{+} population of lung epithelia were significantly reduced in percentage from CD11c^{Cre}TFF2^{flox} mice compared to CD11c^{Cre} mice (Figure 4d), concordant with significantly reduced mRNA expression

levels for *Spc* (encoding surfactant protein C) and *Cc10* (encoding Clara cell 10kDa protein) at d9 (Figure 4e and f). Taken together, these data demonstrate that lack of myeloid-derived TFF2 reduced epithelial proliferation during recovery from bleomycin injury.

Mφ promote epithelial regeneration through a TFF2-dependent mechanism

To determine whether Mφ-driven epithelial proliferation following injury was direct or indirect processes, a co-culture system was developed to isolate the Mφ-epithelial cell interaction *in vitro*. This system, referred to as the macrophage-epithelial repair assay (MERA) utilized primary mouse airway epithelial cells cultured under bi-phasic conditions (i.e. air-liquid interface) in trans-well inserts with bone marrow Mφ (BMMφ) attached to the basolateral surface directly underneath. The two cell populations were separated across a semi-permeable barrier (10 μm thick with pore size 0.4 μm) and evaluated following a pipet-mediated scratch wound to the epithelial monolayer (Figure 5a). Tracheal epithelia were initially used due to the high trans-epithelial cell resistance (TER) levels (generally >1000Ω). As expected, Mφ cultured alone lacked electrical resistance, but epithelia cultured alone maintained TER levels over 1000Ω (Figure 5b).

Upon injury, Mφ significantly accelerated the TER rebound following pipetmediated scratch because Mφ-epithelia co-cultures resulted in 100% restoration of baseline TER levels by d3, further increasing to 130% by d4 post-scratch (Figure 5c). However, in the absence of Mφ, the epithelia only recovered 65% of baseline TER levels by d4 post-injury (Figure 5c). The ability of Mφ to promote TER rebound did not require rIL-4 or rIL-13 administration, nor were any defects in TER recovery observed using IL-4Rα$^{-/-}$ Mφ (Figure 5d). In contrast, using TFF2 deficient Mφ reduced the re-epithelialization rate and resulted in only 4550% TER restoration by d4 post-wounding (Figure 5e). Detectable levels of TFF2 protein were found in MTEC supernatant lacking Mφ, but the presence of Mφ increased supernatant TFF2 levels 2-fold (Figure 5f).

To determine whether epithelial barrier restoration and proliferation were functionally linked, BrdU incorporation was assessed on MTEC harvested on d4 and gated on EpCAM^{+}, junctional adhesion molecule-1 (JAM-1^{+}) cells to ensure evaluation of mature epithelial cells devoid of macrophages (Figure 5g). Of the live EpCAM^{+} cells recovered from the apical side of the transwell insert, (Supplementary Figure 4c), only low levels of epithelial proliferation occurred in cultures lacking Mφ, but the BrdU^{+} epithelial population increased 7-fold with WT Mφ (Figure 5h and i). TFF2$^{-/-}$ Mφ promoted a moderate increase in proliferation over cultures lacking Mφ, but IL-4Rα$^{-/-}$ Mφ stimulated an 8-fold increase in BrdU^{+} epithelia over cultures lacking Mφ (Figure 5j and k). In the absence of Mφ, rTFF2 treatment increased proliferation only 2-fold (Figure 5l and m). Application of rTFF2 alone (without Mφ) significantly accelerated TER rebound over the scratched, mock-treated cultures (Figure 5n). Moreover, WT alveolar macrophages (AM) significantly accelerated TER restoration, but TFF2$^{-/-}$ AM were less able to promote repair, whereas lack of TFF2 within the epithelia impaired TER rebound irrespective of the AM genotype (Figure 5o).

To address whether macrophages also promoted recovery of epithelia population relevant to the distal lung compartment, primary alveolar type 2 (AT2) cells were used instead of MTEC. In this setting, WT Mφ also induced greater EdU incorporation (Figure 5p and q)

and TER recovery (Figure 5r) than TFF2$^{-/-}$ Mφ. Taken together, Mφ induced recovery of epithelial barrier function and also epithelial proliferation through TFF2-dependent mechanism.

Macrophage-derived TFF2 is necessary for myeloid derived non-canonical Wnt expression

To further understand the mechanism acting downstream of TFF2 expression in myeloid cells, RNA-sequencing was completed on WT or TFF2$^{-/-}$ BMMφ recovered from MERA at d4 and compared to reads obtained from naïve BMMφ exposed to quiescent MTEC. TFF2 mRNA transcripts were not different between WT Mφ exposed to intact or damaged epithelia (not shown), but we found that WT Mφ exposed to damaged MTEC up-regulated canonical M2 genes such as: *Mgl2*, *Socs2*, and *Arg1* (Supplementary Figure 5a). However, comparison of RNA transcripts between WT and TFF2$^{-/-}$ Mφ that were both exposed to damaged MTEC revealed that C*amkk2b* expression was significantly (>2-fold) under-represented in TFF2$^{-/-}$ Mφ (Supplementary Figure 5b). Because C*amkk2b* is implicated in the calcium dependent pathway for Wnt glycoprotein expression[34, 35], which in turn regulates multiple aspects of epithelial cell biology, we reasoned that Mφ-derived TFF2 may promote epithelial repair, at least partially, via regulating Wnt expression.

To test this hypothesis, cDNA-derived from different Mφ populations recovered from d4 of MERA were screened against a panel of 84 different Wnt pathway genes. *Wnt4a* and *Wnt16* were 2-fold increased in WT Mφ exposed to damaged epithelia vs. WT Mφ exposed to non-scratched, quiescent epithelia (Figure 6a). Remarkably congruent with our hypothesis, *Wnt4a* and *Wnt16* were both 2–3-fold reduced in *Tff2*$^{-/-}$ Mφ exposed to injured epithelia compared to WT Mφ exposed to injured epithelia (Figure 6b). Inoculation of WT MERA cultures with anti-Wnt4 Ab abrogated the TER rebound compared to control IgG treatment (Figure 6c). Real-time PCR quantification of *Wnt4* and *Wnt16* mRNA transcript levels in CD103^{+} DC, IM, and AM populations FACS-sorted from lung tissues of WT and *Tff2*$^{-/-}$ mice at 4d post *N.b* (Supplementary Figure 3a) confirmed that TFF2 deficiency impaired *Wnt4* expression in AM (Figure 6d and e), but did not alter mRNA expression for *Arg1*, *Retnla* and *Nos2* (Supplementary Figure 5c-e).

To confirm that non-canonical Wnt signaling functioned in the same pathway as TFF2 in the context of *N.b.*-induced lung injury, CD11c^{Cre} and CD11c^{Cre}TFF2^{flox} mice were administered either an rWnt4/Wnt16/R-spondin1 cocktail (1μg) or saline control (vehicle). At d4 post-infection, rWnt4/Wnt16/Rspondin treatment caused a 2-fold increase in the percentage of EpCAM^{+}BrdU^{+}pro-Spc^{+} cell populations recovered from the distal lung compartment of the CD11c^{Cre}TFF2^{flox} mice (Figure 6f and g). No increased BrdU incorporation was noted in R-spondin only treated animals (Supplementary Figure 5f). These data imply that Wnt4/16 act downstream of TFF2 as part of Mφ−driven repair processes that restore damaged epithelia.

Discussion

Lung disorders affect millions worldwide, including sufferers of asthma, allergic rhinitis, bronchitis, COPD, lung cancer, emphysema, and pulmonary fibrosis[2]. Persistent epithelial cell injury caused by smoking, allergens, pollutants, particulates, and pathogens all

predispose towards chronic lung pathology[1]. The prevailing hypothesis is that defective epithelial repair drives lung disease progression[36]. Whereas epithelial-intrinsic mechanisms for regeneration have been a major focus, the question as to whether, and if so, how leukocytes may regulate these processes is less well understood. Mφ seem a likely candidate, but there is debate over whether these cells are necessary for mucosal tissue repair[37]. Herein, we demonstrate that Mφ significantly accelerate the repair of damaged respiratory epithelia in three different experimental systems. Repair of lung injury did not require an intact IL-4Rα, nor did it require the presence of T, B, or ILC subsets, although T regulatory lymphocytes (Treg) can promote lung repair in the context of LPS-induced injury[38]. Also, the mechanism seemed independent of M2 cells or ILC[39], suggesting that stereotyped polarization is only necessary for lung tissue repair in certain contexts. Recently, Lechner et al. reported that lung regeneration post-pneumonectomy did require M2 and ILC2, further indicating the importance of biological context[24]. Instead, our data show Mφ induced epithelia to proliferate through TFF2 production, a cytokine previously considered released only from damaged epithelia. Thus, lung Mφ are an important ancillary source of this critical reparative cytokine.

Mφ reside in virtually every organ, where tissue-specific cues instruct unique transcriptional signatures in resident and emigrant Mφ to facilitate host defense, immunoregulation, and tissue homeostasis[40]. Lung Mφ (AM and IM) have been long recognized as immunosuppressive cells that mediate efferocytosis, and phagocytic clearance of inhaled particles and pathogens. Communication between AM and alveolar epithelia enforces an immunosuppressive lung environment[41], but whether such crosstalk regulates epithelial proliferation remained obscure. AM-derived TGF-β promotes Foxp3^{+}Treg expansion[42], but TGF-β promotes fibrosis and restricts epithelial cell proliferation[43]. Thus, our demonstration that lung Mφ deletion reduced both epithelial proliferation and the rebound in lung function prompted our investigation of Mφ-derived molecules that induced lung repair.

Hookworms damage alveolar architecture during their circuitous migration from skin to GI tract, which is ideal to study infectious lung injury. *N.b.* larvae enter the lung within 24h and cause petechial hemorrhage for 3 days before parasites egress to infest the GI tract[44, 45]. IL-4Rα-driven M2 cells suppress pulmonary IL-17 responses during *N.b* infection[46], but whether Type 2 responses also promoted lung tissue regeneration was unclear. We found that IL-4Rα deficiency did not reduce infection-induced epithelial proliferation or barrier restoration, implying that IL-4Rα-dependent M2 cells were non-essential for these processes. However, RNAseq analysis revealed M2-associated gene induction following exposure to damaged epithelia indicating that Mφ can “sense” tissue damage and undergo prototypical M2 polarization. Hookworm injury induced TFF2 expression within large mononuclear cells in a pattern similar to hemorrhagic spots caused by the larvae. In fact, *Tff2* mRNA transcripts were induced in multiple myeloid populations upon hookworm infection (AM, IM and 103^{+} DC). *Tff2* mRNA expression has been noted in spleen and leukocyte populations and most recently in memory CD4^{+} T cells[21]. Because larvae significantly disrupt alveolar architecture, it is conceivable that replacement of dead/damaged AT1 cells requires proliferative expansion of distal lung progenitors. Although there are technical caveats with the use of flow cytometry and planimetry leaving stereology as the sole approach recommended by the American Thoracic Society for quantitation of

epithelial cell number and potentially ATII expansion[47], we demonstrated that AT2 proliferation was impaired in the context of hookworm injury. Bleomycin-treated CD11c^{Cre}TFF2^{flox} mice had a transient reduction of TFF2 levels, increased lung injury, greater weight loss and defective expansion of AT2 cells as compared to CD11c^{Cre} controls. Defective expansion of AT2 suggests that TFF2 derived from myeloid cells may regulate alveolar cell progenitor biology. In support of this notion, TFF2 transactivates GATA6[48], a transcription factor that drives epithelial stem cell development in the airway[49]. We speculate that lung Mφ enter a regenerative stem cell niche, perhaps with lipofibroblasts[50] similar to how intestinal Mφ reside at stem cell niches of intestinal crypts to facilitate regeneration[51].

Our data show that TFF2 did not drive strong proliferation *per se*, but was required for expression of Mφ-derived Wnt4 and Wnt16. Reconstitution experiments demonstrated that Wnt4/Wnt16 increased AT2 proliferation in CD11c^{Cre}TFF2^{flox} mice, but not the CD11c^{Cre} controls, further suggesting that Wnt production was downstream of TFF2. Wnt signaling serves a major role in lung pulmonary regeneration in the context of development and post-injury[3, 4]. Wnt4 promotes mammalian lung development[52] and induces Wnt16 transcription, suggesting that these molecules work in a concerted manner[53]. Fibroblasts have been shown to exist in a regenerative niche with ATII cells to stimulate Wnt production[54]. Recently it was shown that a sub-population of airway epithelial progenitors within the ATII population are driven to expand under Wnt signaling[55]. However, our study is the first to implicate myeloid derived Wnt production, namely Wnt4 and Wnt16 as an additional mechanism of lung repair. Our results are consistent with data from other systems showing that Mφ-derived Wnt's regulate ocular development, hepatocyte specification, and regeneration of kidney and intestine [13, 56–58].

Mφ-derived regenerative factors may also drive malignant neoplasms. TFF2 is a negative prognostic indicator for certain tumors[59] and although TFF3, rather than TFF2, is an important biomarker of human lung cancer[60], it is plausible that a TFF2/Wnt axis can drive tumor progression. Humans with *TFF2* polymorphisms that disrupt the trefoil domain have enhanced survival rates during cholangiocarcinoma suggesting that TFF2 may augment tumor cell growth or metastasis[61]. Coincidentally, most tumors in cholangiocarcinoma patients contain Wnt-expressing tumor associated macrophages[62]. We propose that autocrine TFF2 induces its own expression[63], promoting *Camkk2b*-dependent non-canonical Wnt production for regeneration of nearby epithelial precursors; a mechanism that drives repair of tissue damage caused by worms and cytotoxicity caused by chemicals.

In summary, we propose that epithelial cell proliferation and epithelial barrier restoration are accelerated by tissue Mφ through a TFF2-dependent mechanism. TFF2, in turn endows Mφ with the ability to produce molecules that include, but are not limited to, non-canonical Wnt's that induce epithelial cells to expand within damaged lung tissue. It is likely that similar mechanisms promote tissue repair at other mucosal surfaces.

Methods

Mouse strains

Tet-DTA mice (B6.Cg-Tg(tetO-DTA)1Gfi/J, CD11c-Cre (B6.Cg-Tg(Itgax-cre)11Reiz/J), CD68-rtTa mice (B6.Cg-Tg(CD68-rtTA2S*M2)3Mpil/Mmjax) were from the Jackson laboratory. C57BL/6 IL-4Rα$^{-/-}$ and TFF2$^{-/-}$ mice have been described previously [9, 22]. *Tff2* conditional knock-out td-Tomato fluorescent reporter mice (Tre-tom) generation in C57BL/6 E/S and FLP recombinase breeding was performed by genOway (Lyon, France). All studies were conducted with mice on the C57BL/6 background bred in house under specific-pathogen free barrier conditions at the San Francisco General Hospital or Univeristyof Pennsylvania vivarium. Mice used in experiments were between 6–12 weeks-old and all procedures were reviewed and approved by Institutional Animal Care and Use Committee at University of California at San Francisco (Protocol# AN109782–01) and the University of Pennsylvania IACUC (Protocol# 805911).

Lung with Nippostrongylus brasiliensis and Bleomycin sulfate

Gender-matched mice between 6–12 weeks old were placed in a plexiglass restrainer and given a subcutaneous inoculation of 600–750 larvae per mouse. Infective stage (L_3) larvae were collected from 7–14-day old copro-cultures maintained in the laboratory at 25C. Parasites were collected with a modified Baermann apparatus and washed three times in sterile PBS containing Penicillin/Streptomycin prior to. For Bleomycin induced lung injury, mice were intratracheally instilled with 8.5 U/Kg of bleomycin sulfate (Millipore) on d0. Body mass was measured daily until the day of euthanasia as indicated in each experiment. To assess BrdU/EdU incorporation in both models, mice were injected i.p. with 2 mg of BrdU or EdU solution (made with PBS) the 1624h before euthanasia.

Tissue macrophage depletion

To deplete lung myeloid cell populations, previously characterized CD68-rtTA and CD68-rtTAxTetO-DTA strains [29] mice were inoculated i.n. with 250 ng of anhydrotetracycline (Sigma-Aldrich, St. Louis, MO) every other day starting four days before *N.b.* infection. Mice treated with equal volume (20 μl) of PBS were used as controls.

Lung cell isolation

To assess lung epithelial cell proliferation, distal lung digestion protocol was modified from work by Chapman et al. [64]. In brief, after cardiac puncture, the lungs were perfused with PBS through the right ventricle to remove blood. Then the lungs were instilled with 1 ml dispase (20U/ml), followed by 0.2 ml 0.1% liquefied low-melting agarose. After the agarose hardened, remove the lung and digest on a shaker for 45 min, then disintegrate the lung with forceps and incubate for another 10 min on the shaker. At the end of incubation, collect cells and pass through 100 micron and 70-micron strainers sequentially in order to obtain single cell suspension for fluorescent antibody staining followed by flow cytometry. For the MERA assay, ATII cell isolation was performed as previously described by Atochina-Vasserman et al. [65]. Mouse lungs were lavaged, perfused and inflated with 0.7 ml dispase (50U/ml, BD Biosciences) then tied off from the trachea. Isolated lungs were incubated 30 min at 37C,

after which individual lobes were dissected away from large airways and mechanically dissociated with a McIlwain tissue chopper (Metrohmm USA, Riverview, FL) then incubate at 37 C for 10 min in MEM+ DNase I (20 μg/ml, Sigma). Cell digests were sequentially passed through 100 μm and 40 μm strainers, followed by 3 rounds of 30 min adhesion on plastic tissue culture dishes to remove fibroblasts and mesenchymal cells. Nonadherent cells were collected and subjected to lineage depletion using Dynabeads™ kits (DC enrichment kit and T cell negative isolation kit, both from Thermo Fisher) to remove $CD45^+$ cells. Recovered cells were cultured in HITES medium (Ham's F12 + 15 mM HEPES +0.8 mM $CaCl_2$ + 1% ITS Universal supplement (BD Biosciences)) with 10% FBS + 50 nM Dexamethasone + 0.1 mM 8-Br-cAMP + 0.1 mM IBMX on matrigel (1:10 dilution)-coated 12-well transwell inserts at 250K/well for 24h followed by the addition of recombinant human KGF (10 ng/ml, Sigma). Cells were cultured for 5–7 days before experiments with fresh media added every other day.

Confocal imaging of lung slices

For vital laser-scanning confocal imaging 400 μm thick sections of lungs were prepared as previously described [31]. Briefly, mice were euthanized using a lethal dose of 1.3% tribromoethanol (Avertin, Sigma-Aldrich) and exsanguinated. Exposed lungs were then intra-tracheally inflated with 1.2 ml of 2.0% low melting temperature agarose (Fisher Scientific) at 37° C, and solidified with cold PBS (8–12°C). The left lobes were isolated, sliced into thick sections (400 μm) with a Leica Vibratome VT1000S, mounted on plastic cover slips using Vetbond (3M), and then imaged on a temperature-controlled stage (Warner Instruments, Hamden, CT) maintained at 37°C, while in constant perfusion with oxygenated (95% O2; 5% CO2) RPMI-1640 without phenol red. Images were acquired using a Nikon A1R microscope equipped with an automated Prior XY stage, following manufacturer's protocol and software, and the parameters described here. For excitation a 5 W, 740–1000 nm tunable MaiTai HP (Newport, Irvine, CA) laser was used. A 20× 0.95 N.A. water-immersion objective (Olympus XLUMPLFLN 20×W) was used, and a spatial resolution of 1.13 μm/pixel was achieved. Two μm Z-depth per plane was used for 3-dimensional imaging. Images were recorded using the galvanometer-based scanning mode. For RFP excitation, 990 nm and a 650/50nm emission band pass were used. Following three five-minute washes in HBSS, slices were mounted on coverslips and then imaged. Images were analyzed using Imaris (Bitplane).

SpO_2 measurement

Blood oxygen levels were measured by MouseOx pulse oximeter from Starr Life Sciences (Oakmont, PA) following the manufacturer's protocol. Lungs were perfused with 10 ml of 1×PBS through the left ventricle to remove blood from the vasculature then inflated and fixed with 10% buffered formalin at 20 mmHg using a commercially available system by Braintree Scientific followed by overnight fixation in 10% neutral buffered formalin for fixation and paraffin embedding prior to histological staining and evaluation.

Real Time PCR and qPCR Array

Total RNA was harvested from tissues or cultured cells using RNeasy Mini kit (QIAGEN, Hilden, Germany). Real-time PCR reactions were run on CFX96 RealTime PCR detection

system (Bio-Rad, Hercules, CA). Gene expression is normalized to *Gapdh* and data were presented as Mean ± SEM from the replicates. The Wnt pathway RT^2 Profiler real-time PCR array, RT^2 First Strand Kit and SYBR® Green qPCR Mastermix were all purchased from Qiagen. Realtime PCR reactions were carried out on Bio-Rad CFX96 system and data were analyzed using the ΔΔCt method as recommended in the manual.

Tracheal epithelial cell culture and MERA

Tracheal tissue was resected and perfused overnight with 0.5% protease (Sigma-Aldrich) in DMEM. On the next day, cells were flushed out and plated onto Matrigel™ (BD Biosciences, Bedford, MA)-coated 12-well Transwell chambers (Corning Inc., Corning, NY) in Ham's F12 and DMEM (1:1), supplemented with insulin (5 mg/ml), transferrin (5 mg/ml), epidermal growth factor (10 ng/ml), dexamethasone (0.1 mM), cholera toxin (10 ng/ml), bovine hypothalamus extract (15 mg/ml), *all-trans* retinoic acid (100 nM), and Rhoassociated protein kinase (ROCK) inhibitor Y27632 (10 mM, STEMCELL Technologies, Cambridge, MA). Cells were kept in a 37° C incubator with 5% CO_2 for one week or until the trans-epithelial resistance (TER) values reached 1000_{Ω}. as determined by Millicell ERS-2 Volt-Ohm meter with the ERSS TX03 adjustable electrode set (both from EMD Millipore). MTECs were switched to an air-liquid interface (ALI) culture condition with MTEC differentiation media (DMEM and F12 (1:1) media supplemented with 100 U/ml penicillin, 100 U/ml streptomycin, 100 nM *all-trans* retinoic acid, and 2% NuSerum (BD Biosciences) for an additional 1–2 weeks. For MERA assays, bone marrowderived hematopoietic cells were cultured in DMEM media supplemented with 10% FCS and culture supernatant of a mouse M-CSF secreting cell line. Three days after the initial plating, non-adherent cells were removed and fresh media were added into the culture. On day 4–6 macrophages were harvested and used in MERA. On the day of MERA experiment, Transwell inserts with MTECs were taken out of the wells and flipped over; macrophages were plated on the side opposite to MTECs and allowed 2 h for attachment at 37° C. At the end of incubation period, the bottom side of inserts was rinsed gently with warm PBS before placed back to the plate. Cells were cultured in MTEC differentiation media (without all-*trans* retinoic acid) plus rMCSF containing supernatant (1:10–1:25) for up to 4 days during MERA. TER was measured daily with Millicell ERS-2 Volt-Ohm meter (EMD Millipore, Billerica, MA). For anti-Wnt4 treatments, a mixture of 20 ug/ml of polyclonal goat antimouse Wnt4 (R&D Systems AF475) and 20 ug/ml of rat anti-mouse Wnt4 IgG2a (R&D Systems MAB475) was added to baso-lateral side of MERA wells on day 0 and day 2 of experiments. As control, a mixture of normal goat IgG (R&D Systems AB-108-C) and rat IgG2a (clone GL117) at the same concentration was added. For BrdU/EdU incorporation assays, cells were treated with 10 μM BrdU/EdU solution 16h before harvesting.

Flow cytometry and immunohistochemistry

All the following antibodies were purchased from BioLegend (San Diego, CA): rat anti-mouse CD31 (clone 390), rat anti-mouse CD45 (30-F11), rat antimouse CD49f/6 integrin (GoH3), rat anti-mouse CD104/4 integrin (346–11A), rat anti-mouse F4/80 (BM8), rat anti-mouse Ly6C (HK1.4),rat anti-mouse Ly6G/Gr1 (RB6–8C5), Ly6C (1A8), and rat anti-mouse CD326/EpCAM (G8.8). Hamster anti-mouse Podoplanin/T1 (eBio8.1.1), rat anti-mouse CD11b (M1/70), hamster anti-mouse CD11c (N418), mouse anti-mouse CD45.1

(A20), rat anti-mouse I-A/I-E (M5/114.15.2), and hamster anti-mouse CD103 (2E7) were purchased from eBioscience (San Diego, CA). Cell viability was determined by LIVE/DEAD® Fixable Aqua Stain (Life Technologies). Rat antimouse Siglec-F (E50–2440) and rat anti-mouse CD45.2 (clone 104) were purchased from BD Biosciences. BrdU staining was performed with BrdU Flow kits from BD Biosciences following manufacturer's protocol. Intracellular staining of SpC was achieved by use of rabbit anti-mouse Pro-SpC (Seven Hills Bioreagents, Cincinnati, OH) in conjunction with fluorescence-labeled donkey anti-rabbit secondary antibody (Jackson ImmunoResearch, West Grove, PA). Flow cytometry was carried out on LSRII or Fortessa (BD Biosciences) with BD FACSDiva software. Flow-based cell sorting was performed using BD FACSAria sorter. For immunohistochemistry, perfused lung tissues were formalin fixed and paraffin embedded and sectioned at 3–5micron thickness. Polyclonal goat anti-mouse Ym1 (R&D Systems,) and rabbit anti-mouse Ki67 (AbCam, Cambridge, MA), with secondary Alexa Fluor 488donkey anti-goat and Cy3-donkey anti-rabbit antibody (both from Jackson ImmunoResearch, West Grove, PA) respectively, were used in co-staining. Hard Set™ mounting medium containing DAPI was purchased from Vector Laboratories (Burlingame, CA). Images were acquired on Leica DM600B microscope with LAS software.

ELISA and BALF total protein

Mouse TFF2 ELISA kit was purchased from United States Biological (Salem, MA). To assess BALF protein level, mouse lungs were lavaged with 1 ml PBS after euthanasia and total protein concentration in BALF was measured using Pierce™ BCA protein assay kit (Thermo Fisher) following the manufacture's protocol.

Recombinant Wnt treatment

All reagents, including carrier-free recombinant mouse Wnt4, human Wnt16 and mouse R-Spondin 1, were purchased from R&D Systems. On the day of *Nippostrongylus* infection, mice were given 300 ng of each recombinant protein or equal volume of sterile PBS intranasally. A second dose of mixed Wnts and R-Spondin 1 were administered on day 2 post-infection.

Statistics

All data points represent biological replicates of experiments analyzed using Prism (GraphPad, La Jolla, CA). Fluorescence microscopy images are representative of 5 different high-power fields (hpf) from 3 wild-type C57BL/6 mice. Mean ± standard error were compared using Student's t-test for two groups and one-way ANOVA for three or more groups with significance determined as $P<0.05$.

Supplementary Material

Refer to Web version on PubMed Central for supplementary material.

Acknowledgements

D.R.H. is supported by NIH (AI095289, GM083204, UO1AI125940) and the Burroughs Wellcome Fund. We thank Dean Sheppard and James Frank for critical comments.

References

1. Whitsett JA, Alenghat T. Respiratory epithelial cells orchestrate pulmonary innate immunity. Nat Immunol 2015; 16(1): 27–35. [PubMed: 25521682]
2. Hogan BL, Barkauskas CE, Chapman HA, Epstein JA, Jain R, Hsia RCC et al. Repair and regeneration of the respiratory system: complexity, plasticity, and mechanisms of lung stem cell function. Cell Stem Cell 2014; 15(2): 123–138. [PubMed: 25105578]
3. Vaughan AE, Brumwell AN, Xi Y, Gotts JE, Brownfield DG, Treutlein B et al. Lineage-negative progenitors mobilize to regenerate lung epithelium after major injury. Nature 2015; 517(7536): 621–625. [PubMed: 25533958]
4. Vaughan AE, Chapman HA. Regenerative activity of the lung after epithelial injury. Biochim Biophys Acta 2013; 1832(7): 922–930. [PubMed: 23219956]
5. Kopf M, Schneider C, Nobs SP. The development and function of lungresident macrophages and dendritic cells. Nat Immunol 2015; 16(1): 3644.
6. Schneider C, Nobs SP, Heer AK, Kurrer M, Klinke G, van Rooijen N et al. Alveolar macrophages are essential for protection from respiratory failure and associated morbidity following influenza virus infection. PLoS Pathog 2014; 10(4): e1004053. [PubMed: 24699679]
7. Edwards JP, Zhang X, Frauwirth KA, Mosser DM. Biochemical and functional characterization of three activated macrophage populations. J Leukoc Biol 2006; 80(6): 1298–1307. [PubMed: 16905575]
8. Mosser DM, Edwards JP. Exploring the full spectrum of macrophage activation. Nat Rev Immunol 2008; 8(12): 958–969. [PubMed: 19029990]
9. Herbert DR, Holscher C, Mohrs M, Arendse B, Schwegmann A, Radwanska M et al. Alternative macrophage activation is essential for survival during schistosomiasis and downmodulates T helper 1 responses and immunopathology. Immunity 2004; 20(5): 623–635. [PubMed: 15142530]
10. Murray PJ, Allen JE, Biswas SK, Fisher EA, Gilroy DW, Goerdt S et al. Macrophage activation and polarization: nomenclature and experimental guidelines. Immunity 2014; 41(1): 14–20. [PubMed: 25035950]
11. Murray PJ, Wynn TA. Protective and pathogenic functions of macrophage subsets. Nat Rev Immunol 2011; 11(11): 723–737. [PubMed: 21997792]
12. Van Dyken SJ, Locksley RM. Interleukin-4- and interleukin-13-mediated alternatively activated macrophages: roles in homeostasis and disease. Annu Rev Immunol 2013; 31: 317–343. [PubMed: 23298208]
13. Saha S, Aranda E, Hayakawa Y, Bhanja P, Atay S, Brodin NP et al. Macrophage-derived extracellular vesicle-packaged WNTs rescue intestinal stem cells and enhance survival after radiation injury. Nat Commun 2016; 7: 13096. [PubMed: 27734833]
14. Yeo EJ, Cassetta L, Qian BZ, Lewkowich I, Li JF, Stefater JA, 3rd et al. Myeloid WNT7b mediates the angiogenic switch and metastasis in breast cancer. Cancer Res 2014; 74(11): 2962–2973. [PubMed: 24638982]
15. Clevers H, Nusse R. Wnt/beta-catenin signaling and disease. Cell 2012; 149(6): 1192–1205. [PubMed: 22682243]
16. Schulte G, Bryja V. The Frizzled family of unconventional G-proteincoupled receptors. Trends Pharmacol Sci 2007; 28(10): 518–525. [PubMed: 17884187]
17. Taupin D, Podolsky DK. Trefoil factors: initiators of mucosal healing. Nat Rev Mol Cell Biol 2003; 4(9): 721–732. [PubMed: 14506475]
18. Aamann L, Vestergaard EM, Gronbaek H. Trefoil factors in inflammatory bowel disease. World J Gastroenterol 2014; 20(12): 3223–3230. [PubMed: 24696606]
19. Taupin DR, Kinoshita K, Podolsky DK. Intestinal trefoil factor confers colonic epithelial resistance to apoptosis. Proc Natl Acad Sci U S A 2000; 97(2): 799–804. [PubMed: 10639160]
20. McBerry C, Egan CE, Rani R, Yang Y, Wu D, Boespflug N et al. Trefoil factor 2 negatively regulates type 1 immunity against Toxoplasma gondii. J Immunol 2012; 189(6): 3078–3084. [PubMed: 22896633]

21. Dubeykovskaya Z, Si Y, Chen X, Worthley DL, Renz BW, Urbanska AM et al. Neural innervation stimulates splenic TFF2 to arrest myeloid cell expansion and cancer. Nat Commun 2016; 7: 10517. [PubMed: 26841680]
22. Wills-Karp M, Rani R, Dienger K, Lewkowich I, Fox JG, Perkins C et al. Trefoil factor 2 rapidly induces interleukin 33 to promote type 2 immunity during allergic asthma and hookworm infection. J Exp Med 2012; 209(3): 607–622. [PubMed: 22329990]
23. Hung LY, Oniskey TK, Sen D, Krummel MF, Vaughan AE, Cohen NA et al. Trefoil Factor 2 Promotes Type 2 Immunity and Lung Repair through Intrinsic Roles in Hematopoietic and Nonhematopoietic Cells. Am J Pathol 2018; 188(5): 1161–1170. [PubMed: 29458008]
24. Lechner AJ, Driver IH, Lee J, Conroy CM, Nagle A, Locksley RM et al. Recruited Monocytes and Type 2 Immunity Promote Lung Regeneration following Pneumonectomy. Cell Stem Cell 2017; 21(1): 120–134 e127. [PubMed: 28506464]
25. Craig JM, Scott AL. Helminths in the lungs. Parasite Immunol 2014; 36(9): 463–474. [PubMed: 25201409]
26. Jenkins SJ, Ruckerl D, Thomas GD, Hewitson JP, Duncan S, Brombacher F et al. IL-4 directly signals tissue-resident macrophages to proliferate beyond homeostatic levels controlled by CSF-1. J Exp Med 2013; 210(11): 2477–2491. [PubMed: 24101381]
27. Jenkins SJ, Ruckerl D, Cook PC, Jones LH, Finkelman FD, van Rooijen N et al. Local macrophage proliferation, rather than recruitment from the blood, is a signature of TH2 inflammation. Science 2011; 332(6035): 1284–1288. [PubMed: 21566158]
28. Nieves W, Hung LY, Oniskey TK, Boon L, Foretz M, Viollet B et al. Myeloid-Restricted AMPKalpha1 Promotes Host Immunity and Protects against IL-12/23p40-Dependent Lung Injury during Hookworm Infection. J Immunol 2016; 196(11): 4632–4640. [PubMed: 27183598]
29. Gheryani N, Coffelt SB, Gartland A, Rumney RM, Kiss-Toth E, Lewis CE et al. Generation of a novel mouse model for the inducible depletion of macrophages in vivo. Genesis 2013; 51(1): 41–49. [PubMed: 22927121]
30. Farrell JJ, Taupin D, Koh TJ, Chen D, Zhao CM, Podolsky DK et al. TFF2/SP-deficient mice show decreased gastric proliferation, increased acid secretion, and increased susceptibility to NSAID injury. J Clin Invest 2002; 109(2): 193–204. [PubMed: 11805131]
31. Thornton EE, Krummel MF, Looney MR. Live imaging of the lung. Curr Protoc Cytom 2012; Chapter 12: Unit12 28.
32. van Rijt LS, Jung S, Kleinjan A, Vos N, Willart M, Duez C et al. In vivo depletion of lung CD11c+ dendritic cells during allergen challenge abrogates the characteristic features of asthma. J Exp Med 2005; 201(6): 981–991. [PubMed: 15781587]
33. Wilson MS, Madala SK, Ramalingam TR, Gochuico BR, Rosas IO, Cheever AW et al. Bleomycin and IL-1beta-mediated pulmonary fibrosis is IL-17A dependent. J Exp Med 2010; 207(3): 535–552. [PubMed: 20176803]
34. Qu F, Wang J, Xu N, Liu C, Li S, Wang N et al. WNT3A modulates chondrogenesis via canonical and non-canonical Wnt pathways in MSCs. Front Biosci (Landmark Ed) 2013; 18: 493–503. [PubMed: 23276938]
35. Wang Q, Symes AJ, Kane CA, Freeman A, Nariculam J, Munson P et al. A novel role for Wnt/Ca2+ signaling in actin cytoskeleton remodeling and cell motility in prostate cancer. PLoS One 2010; 5(5): e10456. [PubMed: 20454608]
36. Wynn TA. Integrating mechanisms of pulmonary fibrosis. J Exp Med 2011; 208(7): 1339–1350. [PubMed: 21727191]
37. Martin P, D'Souza D, Martin J, Grose R, Cooper L, Maki R et al. Wound healing in the PU.1 null mouse--tissue repair is not dependent on inflammatory cells. Curr Biol 2003; 13(13): 1122–1128. [PubMed: 12842011]
38. Mock JR, Garibaldi BT, Aggarwal NR, Jenkins J, Limjunyawong N, Singer BD et al. Foxp3+ regulatory T cells promote lung epithelial proliferation. Mucosal Immunol 2014; 7(6): 1440–1451. [PubMed: 24850425]
39. Monticelli LA, Sonnenberg GF, Abt MC, Alenghat T, Ziegler CG, Doering TA et al. Innate lymphoid cells promote lung-tissue homeostasis after infection with influenza virus. Nat Immunol 2011; 12(11): 1045–1054. [PubMed: 21946417]

40. Lavin Y, Winter D, Blecher-Gonen R, David E, Keren-Shaul H, Merad M et al. Tissue-resident macrophage enhancer landscapes are shaped by the local microenvironment. Cell 2014; 159(6): 1312–1326. [PubMed: 25480296]
41. Westphalen K, Gusarova GA, Islam MN, Subramanian M, Cohen TS, Prince AS et al. Sessile alveolar macrophages communicate with alveolar epithelium to modulate immunity. Nature 2014; 506(7489): 503–506. [PubMed: 24463523]
42. Soroosh P, Doherty TA, Duan W, Mehta AK, Choi H, Adams YF et al. Lung-resident tissue macrophages generate Foxp3+ regulatory T cells and promote airway tolerance. J Exp Med 2013; 210(4): 775–788. [PubMed: 23547101]
43. Siegel PM, Massague J. Cytostatic and apoptotic actions of TGF-beta in homeostasis and cancer. Nat Rev Cancer 2003; 3(11): 807–821. [PubMed: 14557817]
44. Hung LY, Lewkowich IP, Dawson LA, Downey J, Yang Y, Smith DE et al. IL-33 drives biphasic IL-13 production for noncanonical Type 2 immunity against hookworms. Proc Natl Acad Sci U S A 2013; 110(1): 282–287. [PubMed: 23248269]
45. Herbert DR, Yang JQ, Hogan SP, Groschwitz K, Khodoun M, Munitz A et al. Intestinal epithelial cell secretion of RELM-beta protects against gastrointestinal worm infection. J Exp Med 2009; 206(13): 2947–2957. [PubMed: 19995957]
46. Chen F, Liu Z, Wu W, Rozo C, Bowdridge S, Millman A et al. An essential role for TH2-type responses in limiting acute tissue damage during experimental helminth infection. Nat Med 2012; 18(2): 260–266. [PubMed: 22245779]
47. Jansing NL, Patel N, McClendon J, Redente EF, Henson PM, Tuder RM et al. Flow Cytometry Underestimates and Planimetry Overestimates Alveolar Epithelial Type 2 Cell Expansion after Lung Injury. Am J Respir Crit Care Med 2018; 198(3): 390–392. [PubMed: 29533675]
48. Al-azzeh ED, Fegert P, Blin N, Gott P. Transcription factor GATA-6 activates expression of gastroprotective trefoil genes TFF1 and TFF2. Biochim Biophys Acta 2000; 1490(3): 324–332. [PubMed: 10684977]
49. Zhang Y, Goss AM, Cohen ED, Kadzik R, Lepore JJ, Muthukumaraswamy K et al. A Gata6-Wnt pathway required for epithelial stem cell development and airway regeneration. Nat Genet 2008; 40(7): 862–870. [PubMed: 18536717]
50. Barkauskas CE, Cronce MJ, Rackley CR, Bowie EJ, Keene DR, Stripp BR et al. Type 2 alveolar cells are stem cells in adult lung. J Clin Invest 2013; 123(7): 3025–3036. [PubMed: 23921127]
51. Pull SL, Doherty JM, Mills JC, Gordon JI, Stappenbeck TS. Activated macrophages are an adaptive element of the colonic epithelial progenitor niche necessary for regenerative responses to injury. Proc Natl Acad Sci U S A 2005; 102(1): 99–104. [PubMed: 15615857]
52. Caprioli A, Villasenor A, Wylie LA, Braitsch C, Marty-Santos L, Barry D et al. Wnt4 is essential to normal mammalian lung development. Dev Biol 2015; 406(2): 222–234. [PubMed: 26321050]
53. Kim YC, Clark RJ, Pelegri F, Alexander CM. Wnt4 is not sufficient to induce lobuloalveolar mammary development. BMC Dev Biol 2009; 9: 55. [PubMed: 19878558]
54. Nabhan AN, Brownfield DG, Harbury PB, Krasnow MA, Desai TJ. Single-cell Wnt signaling niches maintain stemness of alveolar type 2 cells. Science 2018; 359(6380): 1118–1123. [PubMed: 29420258]
55. Zacharias WJ, Frank DB, Zepp JA, Morley MP, Alkhaleel FA, Kong J et al. Regeneration of the lung alveolus by an evolutionarily conserved epithelial progenitor. Nature 2018; 555(7695): 251–255. [PubMed: 29489752]
56. Lobov IB, Rao S, Carroll TJ, Vallance JE, Ito M, Ondr JK et al. WNT7b mediates macrophage-induced programmed cell death in patterning of the vasculature. Nature 2005; 437(7057): 417–421. [PubMed: 16163358]
57. Boulter L, Govaere O, Bird TG, Radulescu S, Ramachandran P, Pellicoro A et al. Macrophage-derived Wnt opposes Notch signaling to specify hepatic progenitor cell fate in chronic liver disease. Nat Med 2012; 18(4): 572–579. [PubMed: 22388089]
58. Lin SL, Li B, Rao S, Yeo EJ, Hudson TE, Nowlin BT et al. Macrophage Wnt7b is critical for kidney repair and regeneration. Proc Natl Acad Sci U S A 2010; 107(9): 4194–4199. [PubMed: 20160075]

59. Kosriwong K, Menheniott TR, Giraud AS, Jearanaikoon P, Sripa B, Limpaiboon T. Trefoil factors: tumor progression markers and mitogens via EGFR/MAPK activation in cholangiocarcinoma. World J Gastroenterol 2011; 17(12): 1631–1641. [PubMed: 21472131]

60. Qu Y, Yang Y, Ma D, Xiao W. Increased trefoil factor 3 levels in the serum of patients with three major histological subtypes of lung cancer. Oncol Rep 2012; 27(4): 1277–1283. [PubMed: 22246423]

61. Kamlua S, Patrakitkomjorn S, Jearanaikoon P, Menheniott TR, Giraud AS, Limpaiboon T. A novel TFF2 splice variant (EX2TFF2) correlates with longer overall survival time in cholangiocarcinoma. Oncol Rep 2012; 27(4): 1207–1212. [PubMed: 22159958]

62. Boulter L, Guest RV, Kendall TJ, Wilson DH, Wojtacha D, Robson AJ et al. WNT signaling drives cholangiocarcinoma growth and can be pharmacologically inhibited. J Clin Invest 2015; 125(3): 1269–1285. [PubMed: 25689248]

63. Bulitta CJ, Fleming JV, Raychowdhury R, Taupin D, Rosenberg I, Wang TC. Autoinduction of the trefoil factor 2 (TFF2) promoter requires an upstream cis-acting element. Biochem Biophys Res Commun 2002; 293(1): 366–374. [PubMed: 12054609]

64. Chapman HA, Li X, Alexander JP, Brumwell A, Lorizio W, Tan K et al. Integrin alpha6beta4 identifies an adult distal lung epithelial population with regenerative potential in mice. J Clin Invest 2011; 121(7): 2855–2862. [PubMed: 21701069]

65. Atochina-Vasserman EN, Bates SR, Zhang P, Abramova H, Zhang Z, Gonzales L et al. Early alveolar epithelial dysfunction promotes lung inflammation in a mouse model of Hermansky-Pudlak syndrome. Am J Respir Crit Care Med 2011; 184(4): 449–458. [PubMed: 21616998]

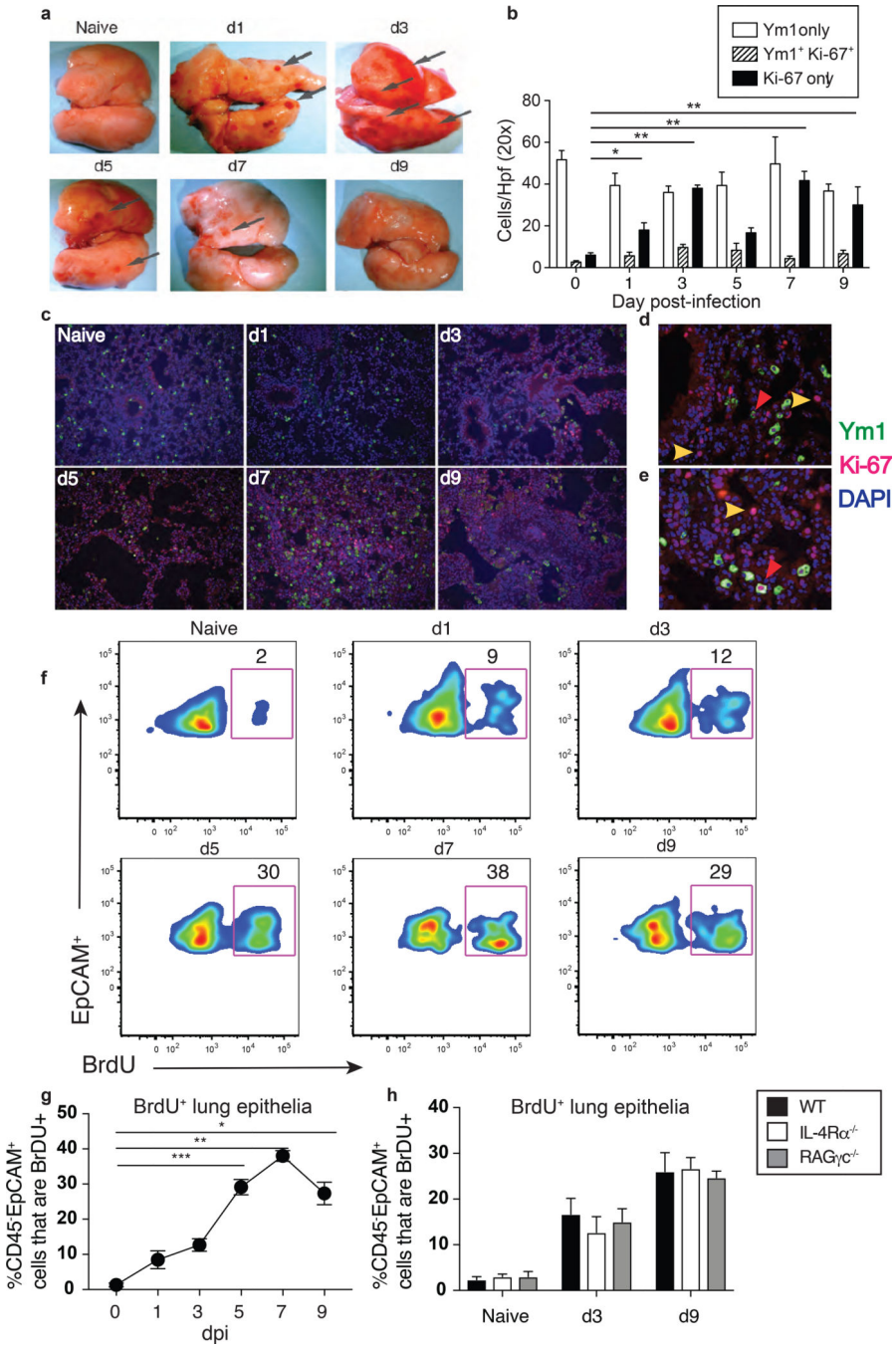

Figure1. Epithelial proliferation after *Nippostrongylus brasiliensis* (*N.b.*) infection.

(**a**) Representative photographs of lung tissues from naive or infected WT C57BL/6 mice at various time-points following subcutaneous infection of 650 L_3 *N.b.*. Arrows point to focal areas of hemorrhagic injury. All images were taken at 20× with Dino-Lite Pro Digital Microscope via Dino Capture 2.0 software. (**b**) Quantifications of $Ym1^+$, $Ym1^+Ki\text{-}67^+$, and $Ki\text{-}67^+$ during *N.b.* infection. For each time-point, 5 randomly selected fields under 20× were counted. (**c**) Kinetic analysis of Ym1 (Cy2) and Ki-67 (Cy3) immunostaining within FFPE distal lung tissues of naïve or *N.b.*-infected mice at the time-points indicated. 200×

magnification. (**d, e**) Images of (**d**) d3 and (**e**) d7 post-infection lung tissues at 400×. Yellow arrowheads indicate Ki-67^{+} cells and red arrowheads indicate Ki67^{+} /Ym1^{+} co-staining, respectively. DAPI counterstain is shown in blue. (**f**) Pseudo-color flow plots showing distal lung total live CD45 neg cells gated for EpCAM^{+} cells that were BrdU^{+} at the indicated time-points following *N.b.* infection. (**g**) Quantification of cells gated as in **f** isolated from WT C57BL/6 mice. (**h**) Comparison of cells gated as in **f** from WT, IL-4Rα$^{-/-}$ and RAGγc$^{-/-}$ strains at indicated time points. N=4 mice/group. Mean ±SEM are shown. *p<0.05, **p<0.01, and ***p<0.005 via ANOVA. Representative data from 3 independent experiments.

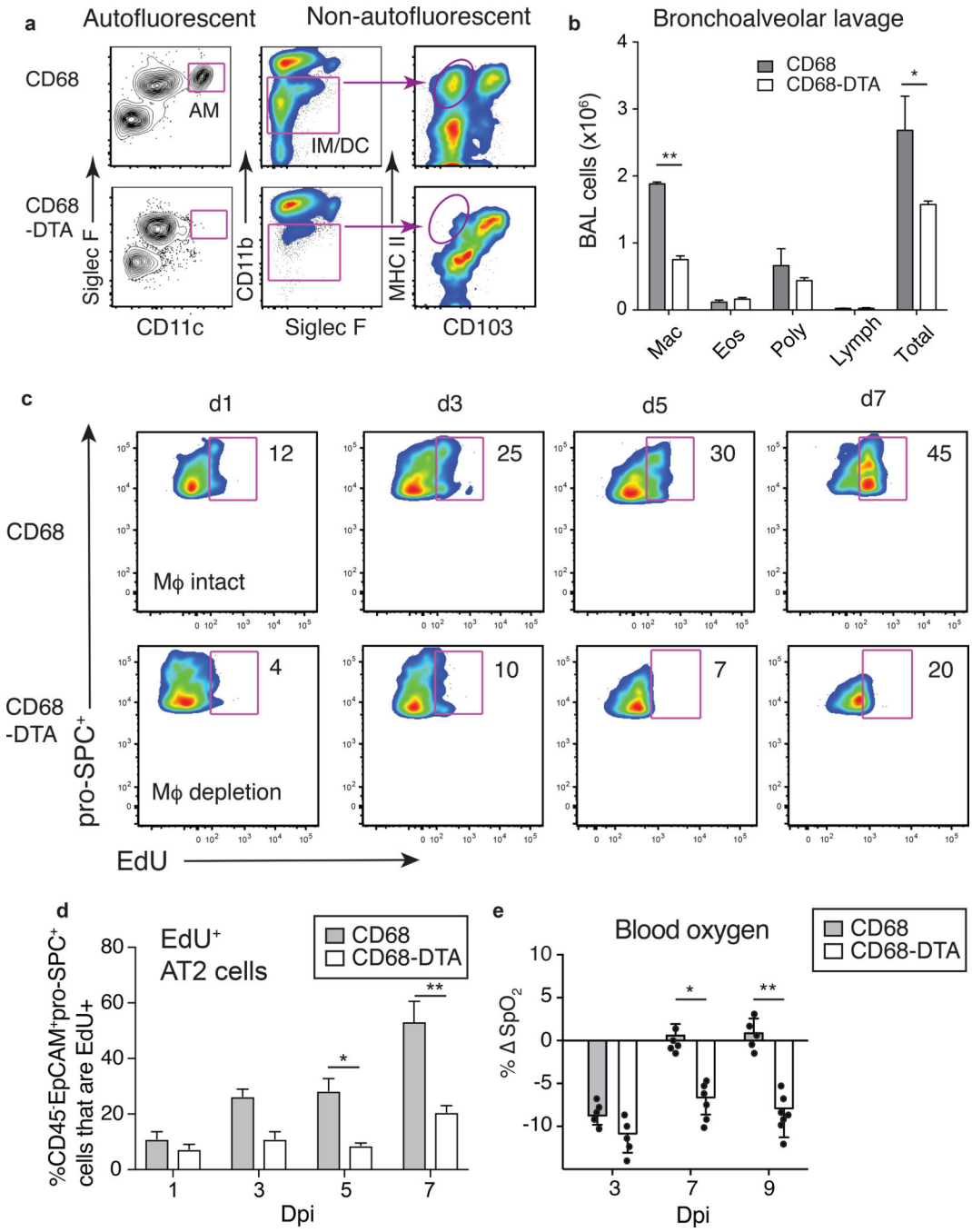

Figure 2. Myeloid cells are required for epithelial proliferation after *N.b.* infection

Anhydrotetracycline (Ahtet) was administered i.n. (250 ng/dose) on d-4, d-2, d0, and d2 of *N.b.* infection protocol: (**a**) Flow cytometry plots showing deletion specificity within whole lung digests and (**b**) Differential counts of cells recovered from bronchoalveolar lavage fluid of CD68-rtTA (CD68) vs. CD68-rtTA-TetO-DTA (CD68-DTA) mice at d4 following *N.b.* infection. (**c**) Representative flow plots and (**d**) quantification total live CD45 neg cells gated for EpCAM^{+} cells that were proSPC+ and BrdU^{+} from CD68 and CD68-DTA lungs on indicated day post *N.b.* infection (Dpi). (**e**) Percent change in blood oxygen content (SpO_2)

normalized to baseline levels at the indicated time-points post- *N.b.* infection (Dpi). Each symbol indicates individual mouse. *p<0.05, **p<0.01 via Student's t test. Mean ±SEM are shown. Representative data from 3 independent experiments.

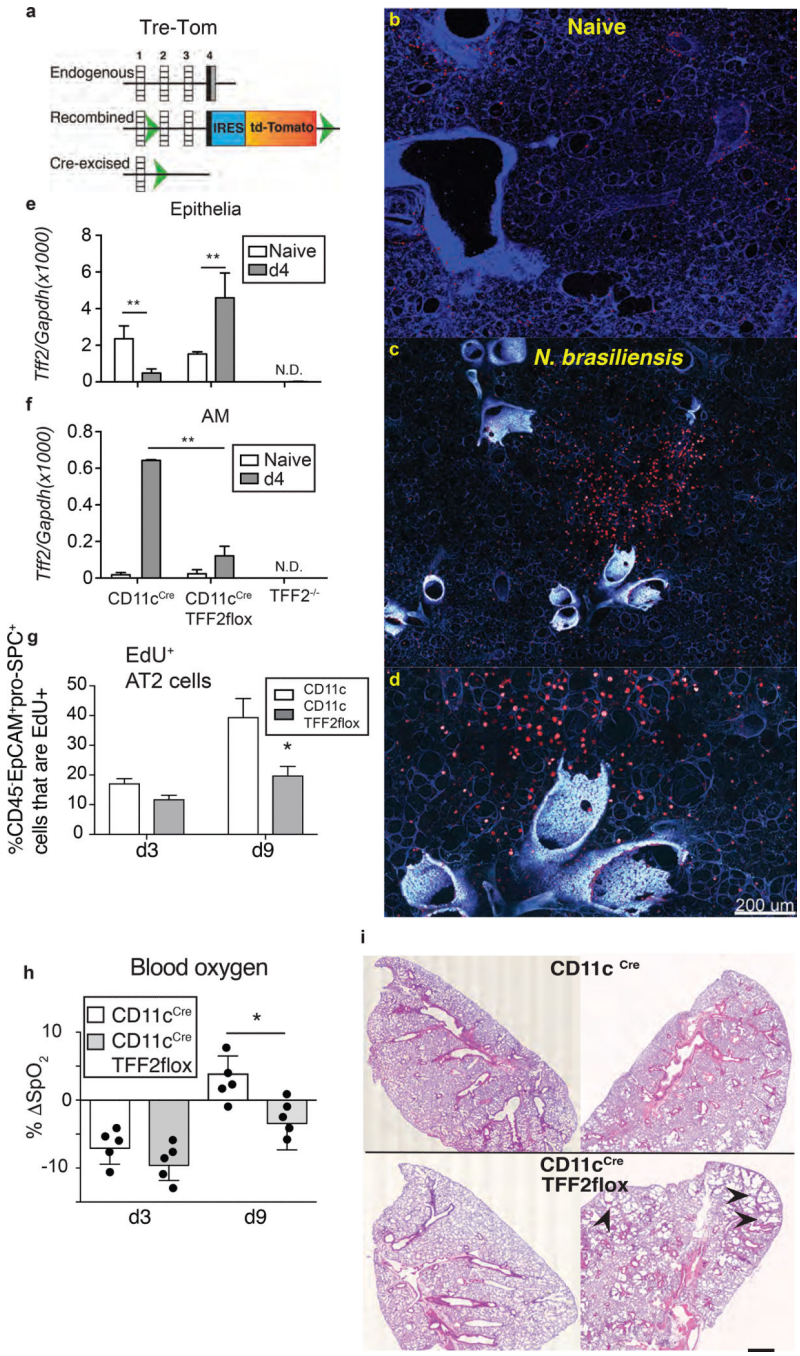

Figure 3. CD11c-specific TFF2 deletion exacerbates lung pathology following *N.b.* -induced injury.

(**a**) Schematic illustration of TFF2-flox/reporter (Tre-Tom) generation. (**b-d**) Confocal microscopy images showing baseline expression of TFF2 in agaroseinflated lung tissues of (**b**) naïve and (**c, d**) *N.b.*-infected TFF2-TdTomato fluorescent reporter (Tre-Tom) mice on d4 at (**c**) 200× and (**d**) 400×. (**e, f**) Quantitative *Tff2* mRNA levels in sorted (**e**) epithelial cells and (**f**) AM from naïve (open bars) or d4 *N.b.*-infected (grey bars) lungs of CD11c^{Cre}, CD11c^{Cre}TFF2^{flox} and TFF2$^{-/-}$ mice. (**g**) Percentages of BrdU^{+} AT2 cells in CD11c^{Cre} vs

$CD11c^{Cre}TFF2^{flox}$ lungs at indicated time-points after *N.b.* infection. (**h**) Change of blood oxygen levels from baseline at d3 and d9 following *N.b.* infection in $CD11c^{Cre}$ and $CD11c^{Cre}TFF2^{flox}$ mice. (**i**) Representative lung pathology of naïve (left) and d9 following *N.b.* infection (right) in $CD11c^{Cre}$ and $CD11c^{Cre}TFF2^{flox}$ mice. Arrowheads indicate emphysematous areas. 20× magnification. *$p<0.05$, **$p<0.01$ determined by ANOVA or Student's t-test. Mean ±SEM are shown.

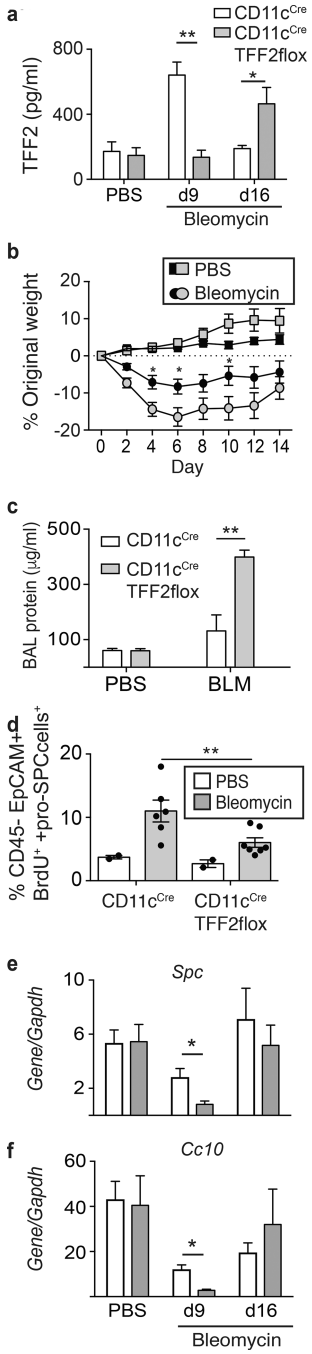

Figure 4. CD11c-specific TFF2 expression is critical for lung epithelial proliferation and recovery from Bleomycin-induced pathology

(**a**) BAL TFF2 levels from PBS-treated or at d9 or d16 after Bleomycin (BLM) treatment in $CD11c^{Cre}$ and $CD11c^{Cre}$-TFF2flox mice. (**b**) Weight changes over two weeks after BLM treatment in $CD11c^{Cre}$ (black symbols) and $CD11c^{Cre}$TFF2flox (grey symbols) mice. (**c**) Total protein levels in BAL from PBS-treated or d9 BLM-treated mice. (**d**) Percentage of BrdU+EpCAM+ cells in the lungs from PBS controls or on d9 after BLM treatment. Each symbol represents individual mouse. (**e**, **f**) Message RNA levels of (**e**) *SpC* and (**f**) *Cc10*

from lungs of PBStreated or d9/d16 BLM-treated $CD11c^{Cre}$ (open bars) or $CD11c^{Cre}$-TFF2flox (grey bars) mice. Mean ±SEM are shown. *p<0.05 and **p< 0.01 as determined by ANOVA or Student's t-test. Representative results from three independent experiments were shown. N=3–6/group unless specified otherwise.

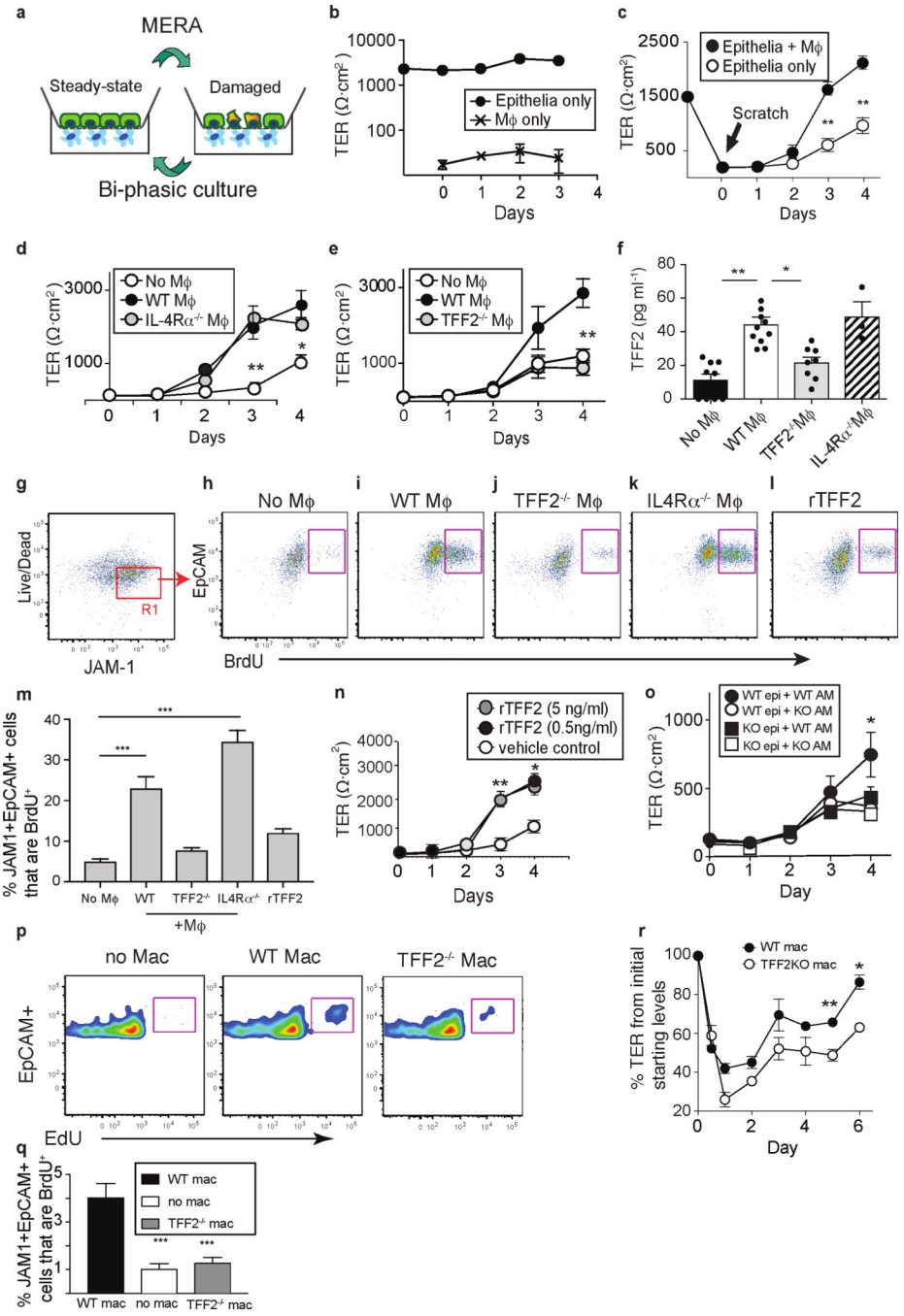

Figure 5. The macrophage-epithelial repair assay (MERA) reveals that macrophage intrinsic TFF2 drives epithelial proliferation and barrier restoration.

(**a**) Schematic showing MERA conceptual design. (**b**) Trans-epithelial resistance (TER) values of transwell inserts containing primary tracheal epithelia or bone marrow macrophages (BMMφ) cultured alone. (**c**) TER values following scratch wounding of epithelia in the presence or absence of WT BMMφ. (**d,e**) TER values following epithelial injury in the presence of (**d**) WT vs. IL-4Rα$^{-/-}$ BMMφ and (**e**) WT vs. TFF2$^{-/-}$ BMMφ. (**f**) Levels of TFF2 in MERA cultures with no BMMφ, WT BMMφ, TFF2$^{-/-}$ BMMφ or IL-4Rα

$^{-/-}$ BMMφ. Symbols represent individual wells. (**g**) Gating strategy to identify live epithelial cells recovered from MERA wells that express junctional adhesion molecule (JAM)-1 (R1). (**h-l**) Representative flow plots showing BrdU incorporation in R1 from "**g**" on d4 postscratch wounding (**h**) in the absence of Mφ or in the presence of (**i**) WT BMMφ, (**j**) TFF2$^{-/-}$ BMMφ, and (**k**) IL-4Rα$^{-/-}$ BMMφ. (**l**) BrdU incorporation on d4 postscratch wounding following treatment with 0.5 ng/ml rTFF2 in the absence of BMMφ. (**m**) Quantification of BrdU^{+} epithelial cells as identified in "**h**" to "**l**". N=36/group. (**n**) TER values after scratch wounding of epithelia in the presence of rTFF2 (0.5 or 5 ng/ml). (**o**) TER values following scratch wounding of WT vs. TFF2KO epithelia in the presence of WT or TFF2KO alveolar macrophages. (**p, q**) MERA using AT2 co-cultured without BMM or with WT vs. TFF2$^{-/-}$ BMM. (**p**) Flow plots and (**q**) quantification of EdU^{+} cells. (**r**) TER values following scratch in wells with WT vs. TFF2$^{-/-}$ BMM. Data represent 2–4 independent experiments. *, $p< 0.05$; **, $p< 0.01$ and ***, $p< 0.005$ as determined by one-way ANOVA or t-test.

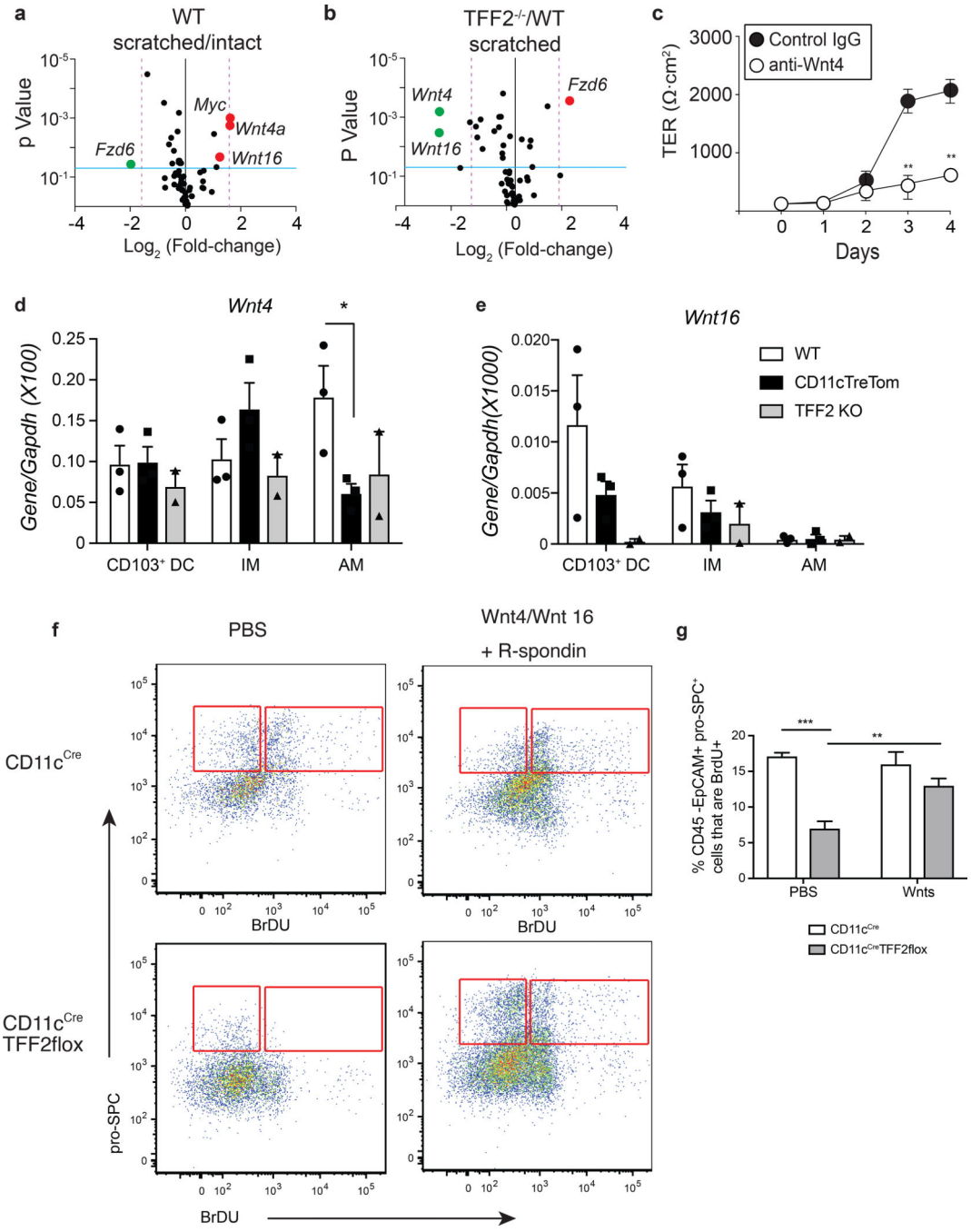

Figure 6. TFF2 is necessary for myeloid-derived non-canonical Wnt4 and Wnt16 expression.

(**a,b**) Volcano plots showing results of a cDNA-based screen for Wnt pathway target genes expressed as the fold-difference between (**a**) WT Mφ exposed to damaged or quiescent epithelia and (**b**) between WT Mφ vs. TFF2$^{-/-}$ Mφ exposed to damaged epithelia. BMMφ were recovered at d4 of MERA for analysis. Each point represents mean of three biological replicates. (**c**) TER values during MERA with WT Mφ in the presence of anti-Wnt4a mAb or control IgG. (**d, e**) Flow-sorted AM, IM and CD103^{+}DC from WT or TFF2 KO lungs at d4 after infection were analyzed for mRNA levels of (**d**) *Wnt4* and (**e**) *Wnt16*. (**f**)

Representative flow plots and (**g**) quantification of $BrdU^+SpC^+$ epithelia from distal lung digest cells pre-gated on the live, $CD45^-$, $EpCAM^+$ population for each designated genotype following i.n. administration of rWnt4/16+ R-Spondin 1 cocktail (1μg/mouse, 2 doses) or saline and analyzed by flow cytometry at d4 following *N.b.* infection (N=5/group). Graphs show Mean±SEM. *, $p<0.05$; **, $p<0.01$ and ***, $p< 0.005$ as determined by ANOVA or Student's t-test.